BNL-99193-2013-TECH
C-A/AP/39;BNL-99193-2013-IR

A Super-Conducting Linac Injector to the BNL-AGS

D. Raparia

February 2001

Collider Accelerator Department
Brookhaven National Laboratory

U.S. Department of Energy
USDOE Office of Science (SC)

DISCLAIMER

C-A/AP/39
February 2001

A Super-Conducting Linac Injector to the BNL-AGS

D. Raparia and A.G. Ruggiero

Collider-Accelerator Department
Brookhaven National Laboratory
Upton, NY 11973

A Super-Conducting Linac Injector to the BNL-AGS*

D. Raparia and A.G. Ruggiero

Brookhaven National Laboratory, PO BOX 5000, Upton, NY 11973
July 31, 2000

Abstract

This paper reports on the feasibility study of a proton Super-Conducting Linac as a new injector to the Alternating Gradient Synchrotron (AGS) of the Brookhaven National Laboratory (BNL). The Linac beam energy is in the range of 1.5 to 2.4 GeV. The beam intensity is adjusted to provide an average beam power of 4 MW at the top energy of 24 GeV. The repetition rate of the Linac-AGS facility is 5 beam pulses per second.

Introduction

It has been proposed to upgrade the Alternating Gradient Synchrotron (AGS) accelerator complex to provide an average proton beam power of 4 MW at the energy of 24 GeV. The facility can be used either as a proton driver for the production of intense muon and neutrino beams, or/and as a pulsed high-energy spallation neutron source. The upgrade requires operation of the accelerator at the rate of five cycles per second, and a new injector for an increase of the AGS beam intensity by a factor of three.

In a separate technical report [1] we have described the methods and the requirements to operate the Brookhaven AGS accelerator facility at the rate of 5 proton beam pulses per second. The major requirement is an extensive addition and modification of the present power supply system. Also other components, notably the accelerating rf cavity system, will have to be substantially modified to allow a six-fold increase of the acceleration rate. At the same time, a new injector to the AGS, capable to operate at the rate of 5 beam pulses per second, and to provide a three-fold increase of the present beam intensity, is required. The present injector made of the 200-MeV Linac and of the 1.5-GeV AGS-Booster will not be able to fulfill the goals of the upgrade.

The proposed new injector, described in this technical report, is a 1.5 - 2.4 GeV Super-Conducting Linac (SCL) with an average output beam power of 250 - 400 kW. The largest energy is determined by the capability to limit beam losses due to stripping of the negative ions that are used for multi-turn injection into the synchrotron. The high-energy case is to be preferred if one wants to reduce the effects of space charge, and to accommodate adequately the beam transverse size in the aperture of the accelerator. The duty cycle is about a half percent. The operation frequency has been chosen to be 805 MHz.

The paper describes the preliminary design of the Super-Conducting Linac. It is composed of three parts; a front end, that is a 60-mA negative-ion source, followed by a 5-MeV RFQ, a room temperature Drift -Tube Linac (DTL) that accelerates protons to 150 MeV, and the Super-Conducting Linac proper (SCL). This in turn is made of four

* Work performed under the auspices of the US Department of Energy.

sections, each with its own energy range, and different cavity-cryostat arrangement. The four sections are labeled: Low-Energy (LE), Medium Low-Energy (MLE), Medium High-Energy (MHE), and High-Energy (HE).

The New Injector

The two different Linac energy cases are compared in Table 1. AGS performance during multi-turn injection is also summarized in the same Table. Both cases correspond to the same average beam current of 0.17 mA, that yields the same average beam power of 4 MW at the top energy of 24 GeV. The repetition rate of 5 beam pulses per second is assumed in both cases; that gives the same intensity of 2.1×10^{14} protons accelerated per AGS cycle; that is a factor of 3 higher then the intensity routinely obtained with the present injector. At the end of injection, that takes about 317-330 turns, the space-charge tune depression is $\Delta\nu = 0.4$ at the energy of 1.5 GeV, and $\Delta\nu = 0.2$ at 2.4 GeV, assuming a bunching factor (the ratio of beam peak current to average current), during the early part of the acceleration cycle, of 4. Also, with the same normalized beam emittance of 250 π mm-mrad, the actual beam emittance is smaller at 2.4 GeV, $\varepsilon = 73\ \pi$ mm-mrad, versus 104 π mm-mrad at 1.5 GeV. Obviously, the effective acceptance of the AGS at injection is to be larger than these beam emittance values.

The front-end of the Linac is made of an ion source operating with a 1% duty cycle at the repetition rate of 5 pulses per second. The beam current within a pulse is 60 mA of negative-hydrogen ions. The ion source seats on a platform at 35-60 kVolt, and is followed by a 5-MeV RFQ that works at 402.5 MHz. The beam is pre-chopped by a chopper located between the ion source and the RFQ. The beam chopping extends over 75% of the beam length, at a frequency matching the accelerating rf (4.11-4.28 MHz) at injection into the AGS. Moreover, the transmission efficiency through the RFQ is taken conservatively to be 80%, so that the average current of the beam pulse in the Linac, where we assume no further beam loss, is 36 mA.

The combination of the chopper and of the RFQ pre-bunches the beam with a sufficiently small longitudinal extension so that each of the beam bunches at 402.5 MHz can be entirely fitted in the accelerating rf buckets of the following DTL that operates at either 402.5 or 805 MHz. The DTL is a room temperature conventional Linac that is not discussed here, except noting that the beam energy in exit is 150 MeV.

The Super-Conducting Linac (SCL)

The Super-Conducting Linac (SCL) accelerates the proton beam from 150 MeV to 1.5 or 2.4 GeV. The configuration and the design procedure of the SCL is described in detail in [2]. It is typically a sequence of a number of identical periods as shown in Figure 1. Each period is made of a cryo-module of length L_{cryo} and of an insertion of length L_{ins}. The insertion is needed for the placement of focusing quadrupoles, vacuum pumps, steering magnets, beam diagnostic devices, bellows and flanges. It can be either at room temperature or in a cryostat as well. Here we assume that the insertions are at room temperature. The cryo-module includes M identical cavities, each of N identical cells, and

each having a length NL_{cell}, where L_{cell} is the length of a cell. Cavities are separated from each other by a drift space d. An extra drift of length L_w may be added internally on both sides of the cryo-module to provide a transition between cold and warm regions. Thus,

$$L_{cryo} = MN L_{cell} + (M-1)\, d + 2 L_w \qquad (1)$$

Table 1. Injector and AGS Parameters for the Upgrade

Linac Average Power, MW	0.25	0.40
Kinetic Energy, GeV	1.5	2.4
β	0.9230	0.9597
Momentum, GeV/c	2.2505	3.2037
Magnetic Rigidity, T-m	7.5068	10.6862
Repetition Rate, Hz	5	5
Average Current, mA	0.1667	0.1667
Tot. Number of Protons	2.0833×10^{14}	2.0833×10^{14}
AGS Circumference, m	807.12	807.12
Revol. Frequency, MHz	0.3428	0.3565
Revolution Period, μs	2.9169	2.8053
Bending Radius	79.832	79.832
Injection Field	0.9403	1.3386
Ion Source Current, mA	60	60
RFQ Transmission, %	80	80
Chopping Ratio, %	75	75
Peak Current, mA	48	48
Average Current, mA	36	36
Protons per Turn	6.563×10^{11}	6.312×10^{11}
Number of injected Turns	317	330
Beam Pulse Length, ms	0.9259	0.9259
Duty Cycle, %	0.4630	0.4630
Bunching Factor	4	4
Norm. Emitt., π mm-mrad	250	250
Emittance, π mm-mrad	104.	73.
Space- Charge Δν	0.41	0.21

There are two symmetric intervals: a minor one, between the two middle points A and B, as shown in Figure 1, that is the interval of a cavity of length $N L_{cell} + d$; and a major one, between the two middle points C and D, that defines the range of a period of total length $L_{cryo} + L_{ins}$. Thus, the topology of a period can be represented as a drift of length g, followed by M cavity intervals, and a final drift of length g, where

$$g = L_w + (L_{ins} - d)/2 \qquad (2)$$

The choice of cryo-modules with identical geometry, and with the same cavity/cell configuration, is economical and convenient for construction. But there is,

nonetheless, a penalty due to the reduced transit-time-factors when a particle crosses cavity cells, with length adjusted to a common central value β_0 that does not correspond to the particle instantaneous velocity. To minimize this affect the SCL is divided in four sections, each designed around a different central value β_0, and, therefore, with different cavity/cell configuration. The cell length in a section is fixed to be

$$L_{cell} = \lambda\beta_0 / 2 \qquad (3)$$

where λ is the rf wavelength. We assume the same operating frequency of 805 MHz for the entire SCL, so that $\lambda = 37.24$ cm. The major parameters of the four sections of the SCL are given in Tables 2 and 3. The cost estimate (with no contingency) for each section of the SCL has been made assuming the cost and rf parameters shown in Table 4. The total expected cost is around 300 M$, including also the front-end and the room-temperature DTL.

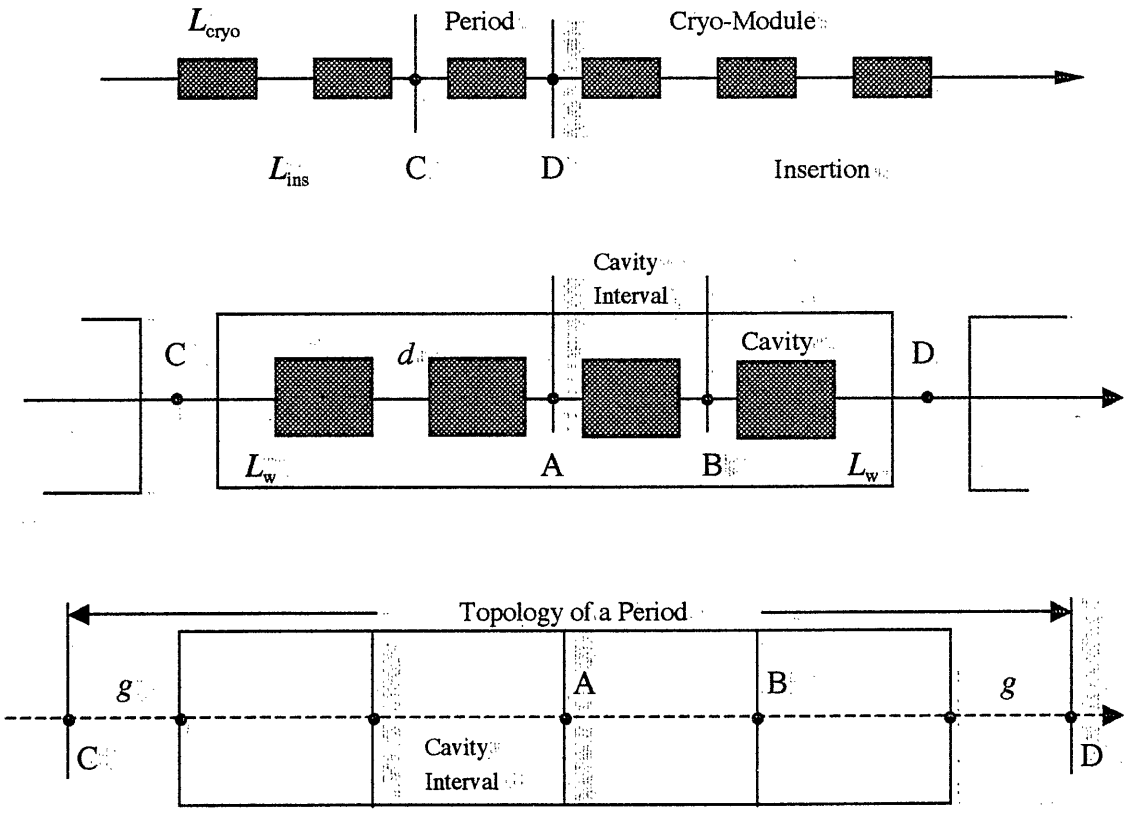

Figure 1. Configuration of a Proton Super-Conducting Linear Accelerator

The length of the Linac depends on the average accelerating gradient. The local gradient has a maximum value that is limited by three causes: (1) The surface field limit at the frequency of the 805 MHz is 26 MV/m. For a realistic cavity shape, we set a limit of a 13 MV/m on the axial electric field. (2) There is a limit on the power provided by rf couplers that we take here not to exceed 400 kW, including a contingency of 50% to

avoid saturation effects. (3) To make the longitudinal motion stable, we can only apply an energy gain per cryo-module that is a relatively small fraction of the beam energy in exit of the cryo-module. The conditions for stability of motion have been derived in [2].

The proposed mode of operation is to operate each section of the SCL with the same rf input power per cryo-module. This will result to some variation of the actual axial field from one cryo-module to the next. If one requires also a constant value of the axial field, this may be obtained by adjusting locally the value of the rf phase. The number of cells and cavities varies from insertion to insertion. The number of couplers varies for 1 to 2. The total length of the injector including the front-end and the DTL is expected to be about 500 meters. The location of the new injector is shown in Figure 2. It runs at an angle of about 30° on the side of the present 200-MeV Linac.

It is proposed to build the entire SCL in two stages. During the first stage the final energy if 1.5 GeV, and the Linac is made of the three first sections. In a second stage the High-Energy section is added for the final energy of 2.4 GeV, if indeed this should result to be necessary.

Table 2. General Parameters of the SCL

Linac Section	LE	MLE	MHE	HE
Average Beam Power, kW	50	133	250	400
Average Beam Current, mA	0.167	0.167	0.167	0.167
Initial Kinetic Energy, GeV	0.150	0.300	0.800	1.500
Final Kinetic Energy, GeV	0.300	0.800	1.500	2.400
Frequency, MHz	805	805	805	805
No. of Protons / Bunch x 10^8	3.73	3.73	3.73	3.73
Temperature, °K	2.0	2.0	2.0	2.0
Cells / Cavity	4	4	4	4
Cavities / Cryo-Module	4	8	8	8
Cavity Separation, cm	32	32	32	32
Cold-Warm Transition, cm	30	30	30	30
Cavity Internal Diameter, cm	10	10	10	10
Length of Warm Insertion, m	1.079	1.079	1.079	1.079
Accelerating Gradient, MeV/m	12.2	11.9	12.9	12.4
Cavities / Klystron	4	8	4	4
No. of rf Couplers / Cavity	1	1	2	2
Rf Phase Angle	30°	30°	30°	30°
Method for Transverse Focussing	FODO	FODO	FODO	FODO
Betatron Phase Advance / FODO cell	90°	90°	90°	90°
Norm. rms Emittance, π mm-mrad	0.30	0.30	0.30	0.30
Rms Bunch Area, π °MeV	0.5	0.5	0.5	0.5

Negative ion stripping during transport down the SCL has been found to be very negligible. But the final 30° bend, before injection into the AGS, could be of a concern [3]. To control the rate of beam loss by stripping to a 10^{-4} level, the bending field should not exceed 2.6 kGauss over a total integrated bending length of 15 m, in the case of the

lower beam energy of 1.5 GeV. At the energy of 2.4 GeV the bending field is 1.9 kGauss, and the integrated bending length is about 30 m.

Table 3. Summary of the SCL Design

Linac Section	LE	MLE	MHE	HE
Energy: in - out, GeV	0.15 - 0.30	0.30 – 0.80	0.80 – 1.50	1.50 – 2.40
Velocity, β: in	0.5066	0.6526	0.8418	0.9230
out	0.6526	0.8418	0.9230	0.9597
Cell Reference β_0	**0.530**	**0.680**	**0.850**	**0.935**
Cell Length, cm	9.87	12.66	15.83	17.41
Total No. of Periods	9	12	13	15
Length of a period, m	4.218	7.971	8.984	9.490
FODO-Cell ampl. func., β_Q, m	14.40	27.21	30.67	32.40
Total Length, m	*37.96*	*95.65*	*116.79*	*142.35*
Coupler rf Power, kW (*)	300	375	255	270
Energy Gain/Period, MeV	16.67	41.67	56.67	60.00
Total No. of Klystrons	9	12	26	30
Klystron Power, kW (*)	1200	3000	2040	2160
$Z_0T_0^2$, ohm/m	271.8	447.4	699.0	845.8
Q_0 x 10^9	5.5	7.0	8.7	9.6
Ave. Dissipated Power, kW	0.009	0.012	0.009	0.008
Ave. HOM-Power, kW	0.0016	0.0042	0.0046	0.0053
Ave. Cryogenic Power, kW	0.152	0.430	0.527	0.644
Ave. Beam Power, MW	0.025	0.083	0.117	0.150
Total Ave. rf Power, MW (*)	0.050	0.149	0.197	0.248
Ave. AC Power for rf, MW (*)	0.110	0.331	0.438	0.552
Ave. AC Power for Cryo., MW	0.038	0.107	0.132	0.161
Total Ave. AC Power, MW (*)	0.148	0.439	0.570	0.713
Efficiency, % (*)	16.9	19.0	20.5	21.0
Capital Cost '00 M$:				
Rf Klystron (*)	0.124	0.373	0.493	0.621
Electr. Distr. (*)	0.021	0.061	0.080	0.100
Refrig. Plant	0.303	0.860	1.055	1.288
Warm Structure	1.619	2.104	2.266	2.590
Cold Structure	14.126	41.351	51.381	63.085
Tunnel	3.904	9.673	11.787	14.343
Total Cost, '00 M$ (*)	20.096	54.422	67.061	82.027
Operation Cost, '00 M$/y (*)	0.049	0.144	0.187	0.234

(*) Including 50% rf power contingency.

A Super-Conducting Linac is most advantageous for a continuous mode of operation (CW). There are two problems in the case of the pulsed-mode of operation. First, the pulsed thermal cycle introduces Lorentz forces that deform the cavity cells out of

resonance. This can be controlled with a thick cavity wall strengthened to the outside by supports. Second, there is an appreciable period of time to fill the cavities with rf power before the maximum gradient is reached [2]. During the filling time, extra power is dissipated also before the beam is injected into the Linac. The extra amount of power required is the ratio of the filling time to the beam pulse length. The filling time is 0.30ms for the LE section, 0.18 ms for the MLE section, 0.12 ms for the MHE section, and 0.10 ms for the HE section. In comparison, the beam pulse length is 0.93 ms.

Table 4. Cost ('00 $) and Other Parameters

AC-to-rf Efficiency	0.45	For pulsed mode
Cryogenic Efficiency	0.004	At 2.0 °K
Electricity Cost	0.05	$ / kWh
Linac Availability	75	% of yearly time
Normal Conducting Cost	150	k$ / m
Superconducting Cost	500	k$ / m
Tunnel Cost	100	k$ / m
Cost of Klystron	2.50	$ / W of rf Power
Cost of Refrigeration Plant	2	k$ / W of Power @ 2.0 °K
Cost of Electrical Distribution	0.14	$ / W of AC Power

A program [4] was written in Visual Basic included with the MS Excel application, to calculate the beam and rf dynamics during acceleration in each of the four sections of the SCL. The results are displayed in Figures 3 to 14.

References

[1] I. Marneris and A.G. Ruggiero, "Running the AGS MMPS at 5 Hz, 24 GeV". BNL-Internal Report C-A/AP/12. January 21, 2000.

[2] A. G. Ruggiero, "Design Considerations on a Proton Superconducting Linac". BNL-Internal Report 62312. August 1995.

[3] A. G. Ruggiero, "Negative-Ion Injection by Charge Exchange at 2.4 GeV". BNL-Internal Report 62310. September 1995.

[4] The program is available by making request to one of the Authors.

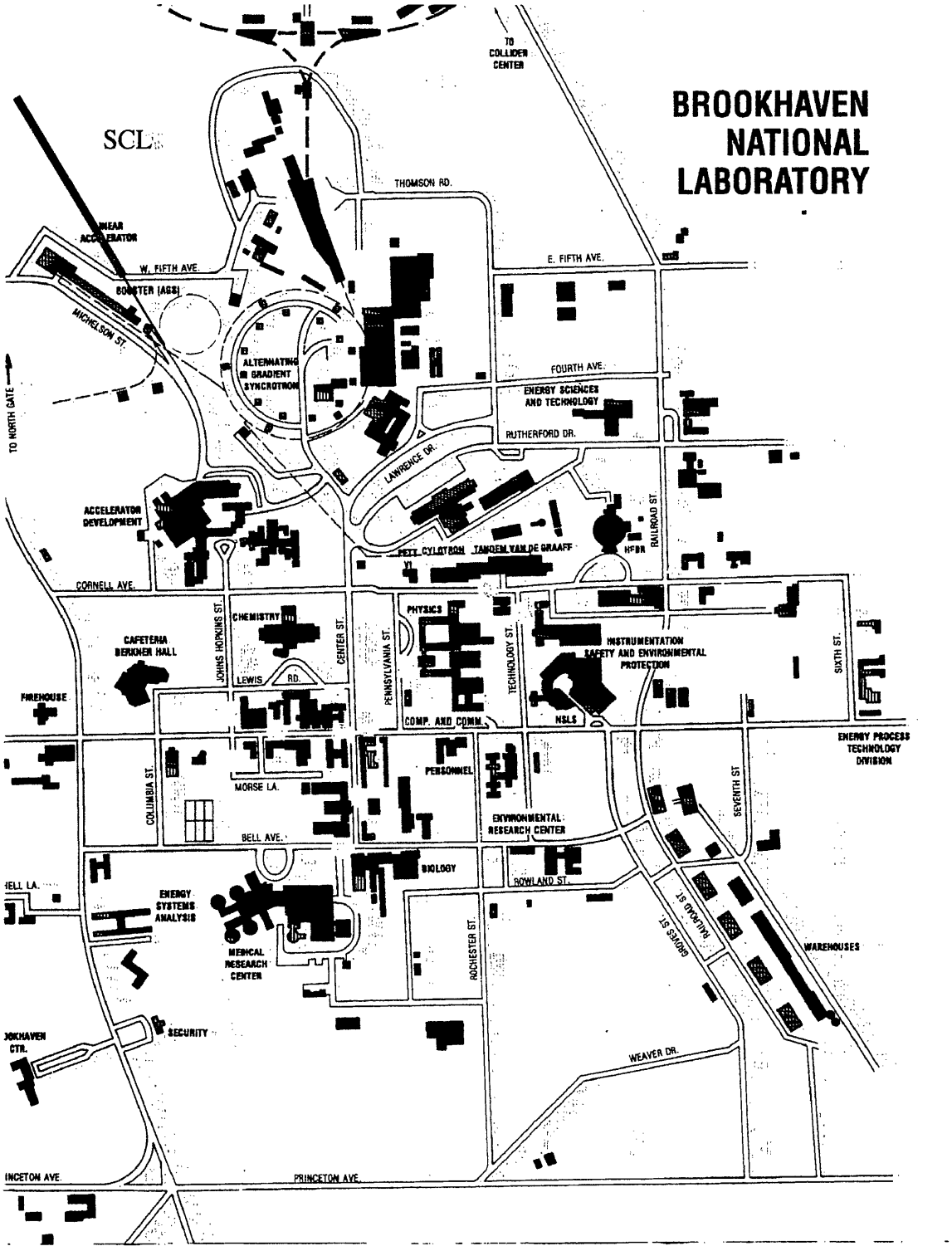

Figure 2. BNL Site with the SCL Injector and the AGS Facility

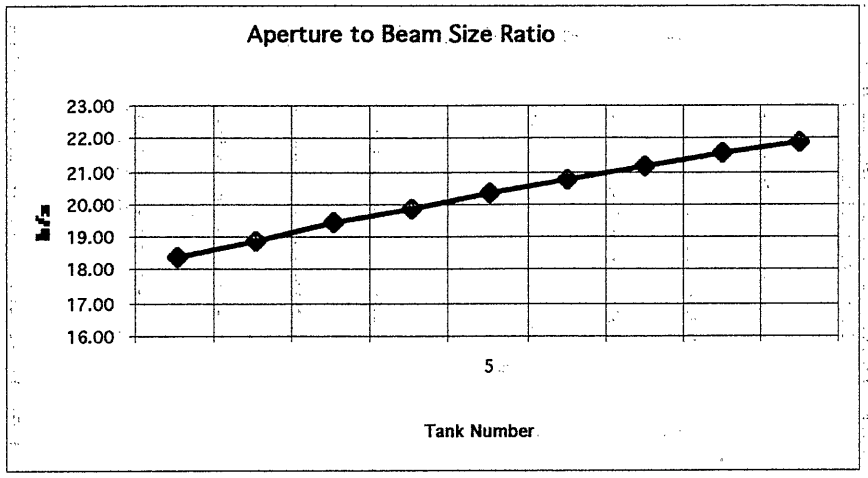

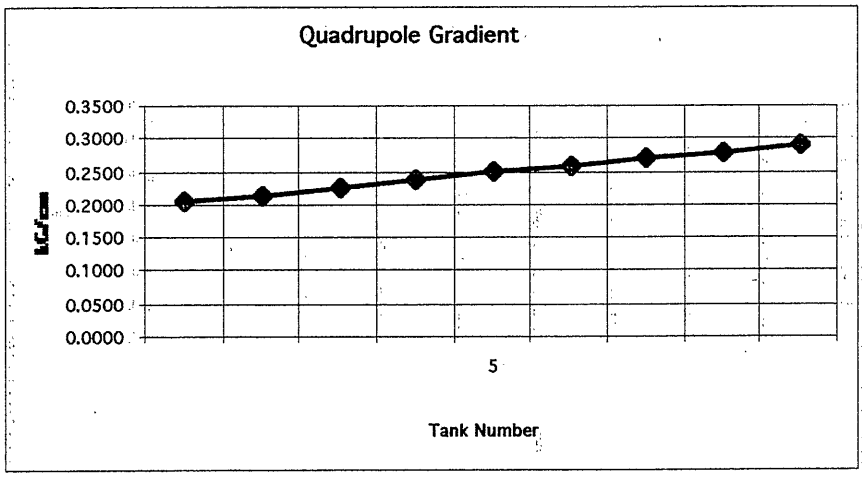

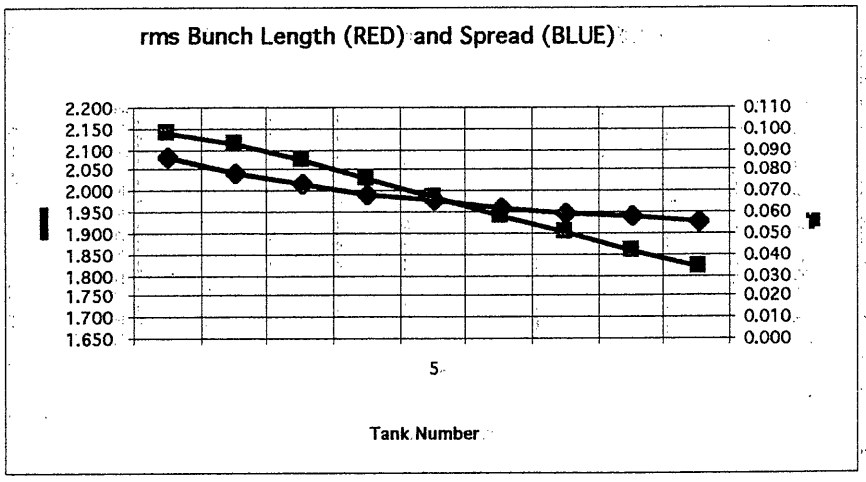

Figure 3. Plots (1) of Behavior vs. *period* (tank) number of LE Section.

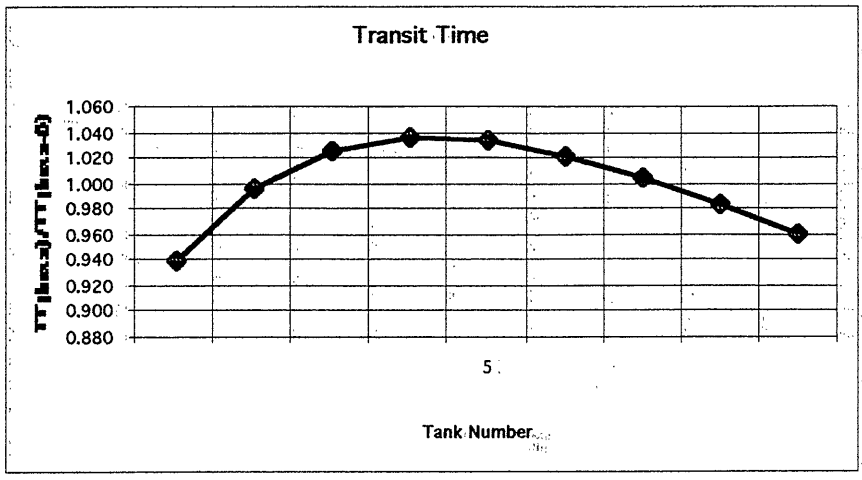

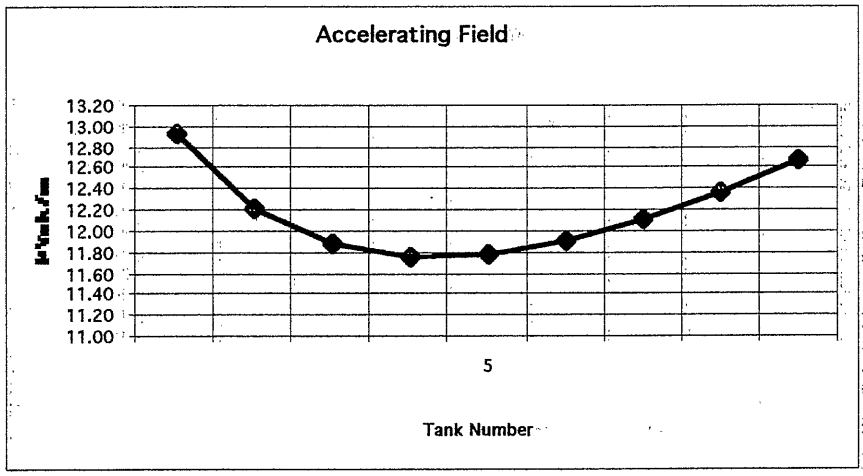

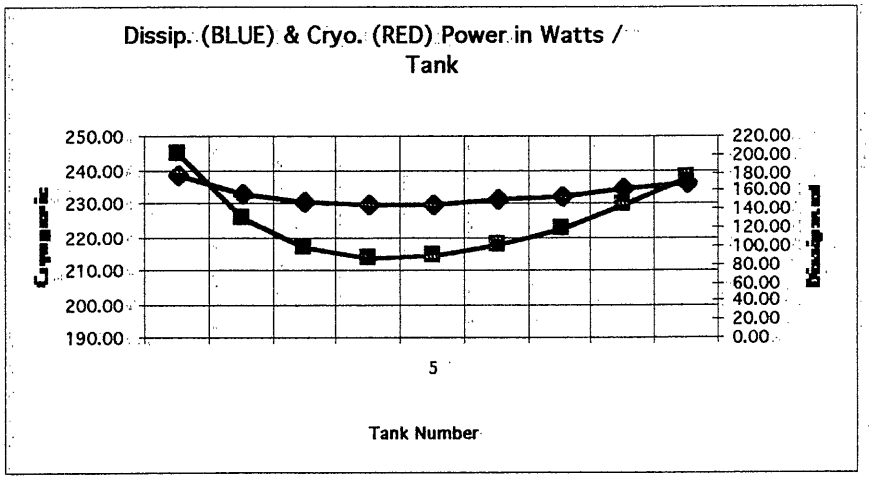

Figure 4. Plots (2) of Behavior vs. *period* (tank) number of LE Section.

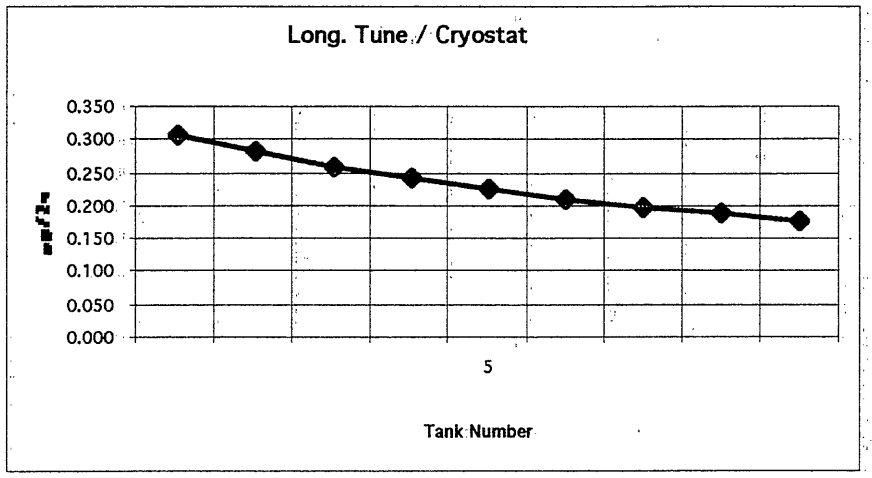

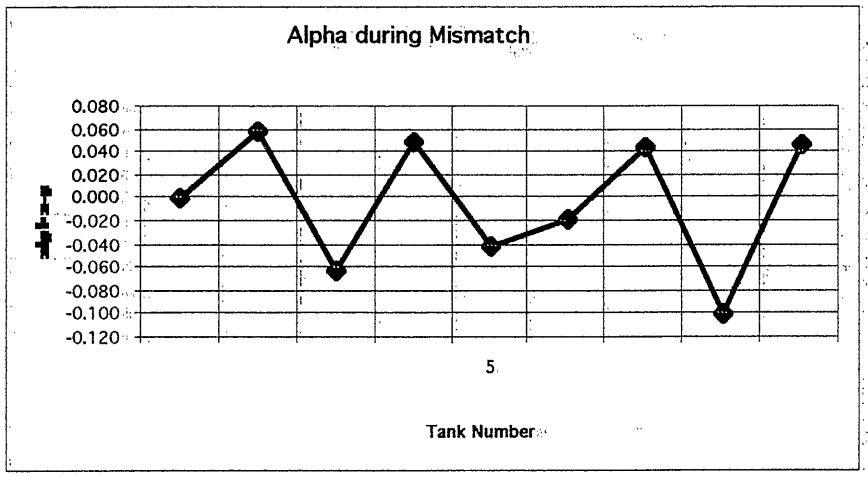

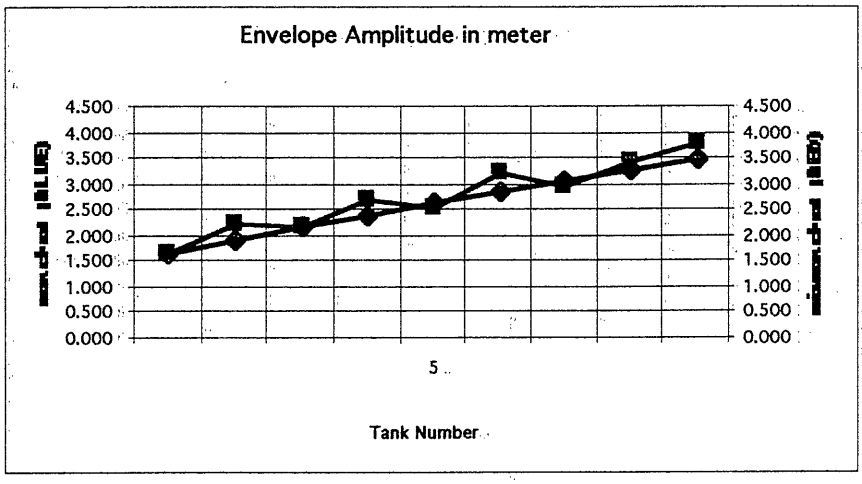

Figure 5. Plots (3) of Behavior vs. *period* (tank) number of LE Section.

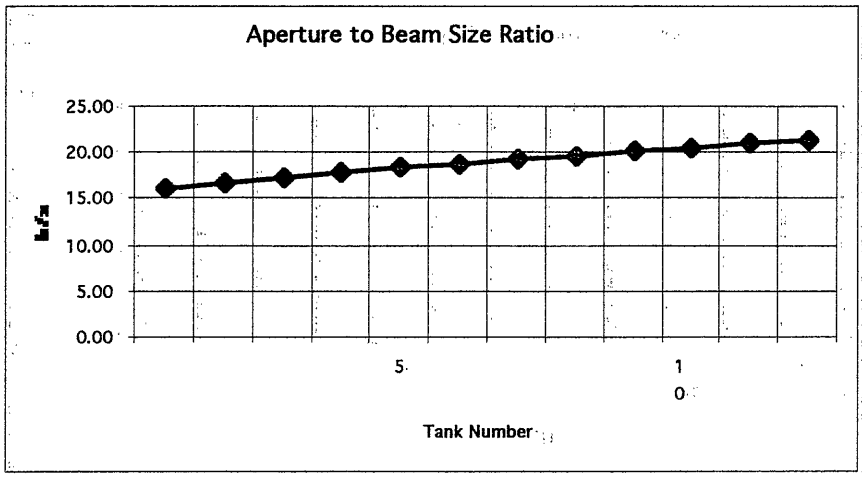

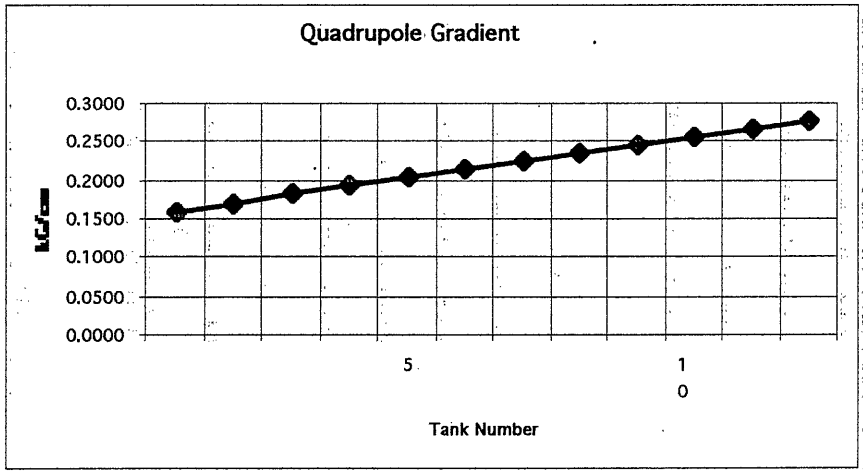

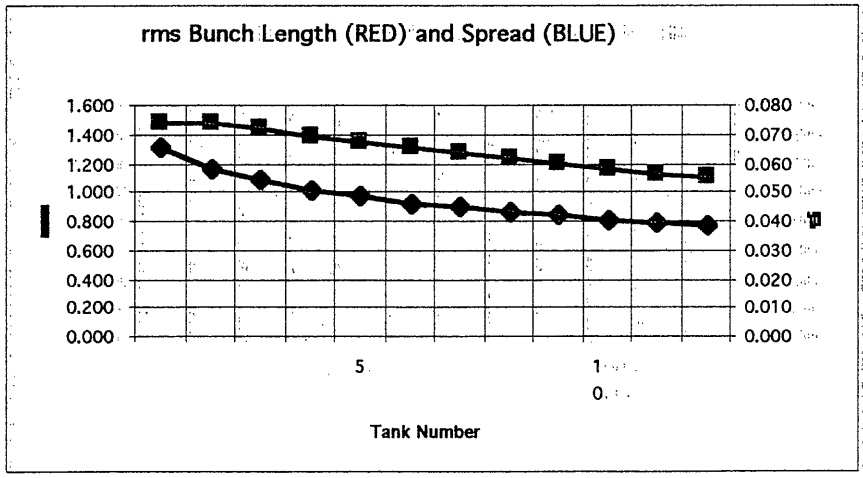

Figure 6. Plots (1) of Behavior vs. *period* (tank) number of MLE Section.

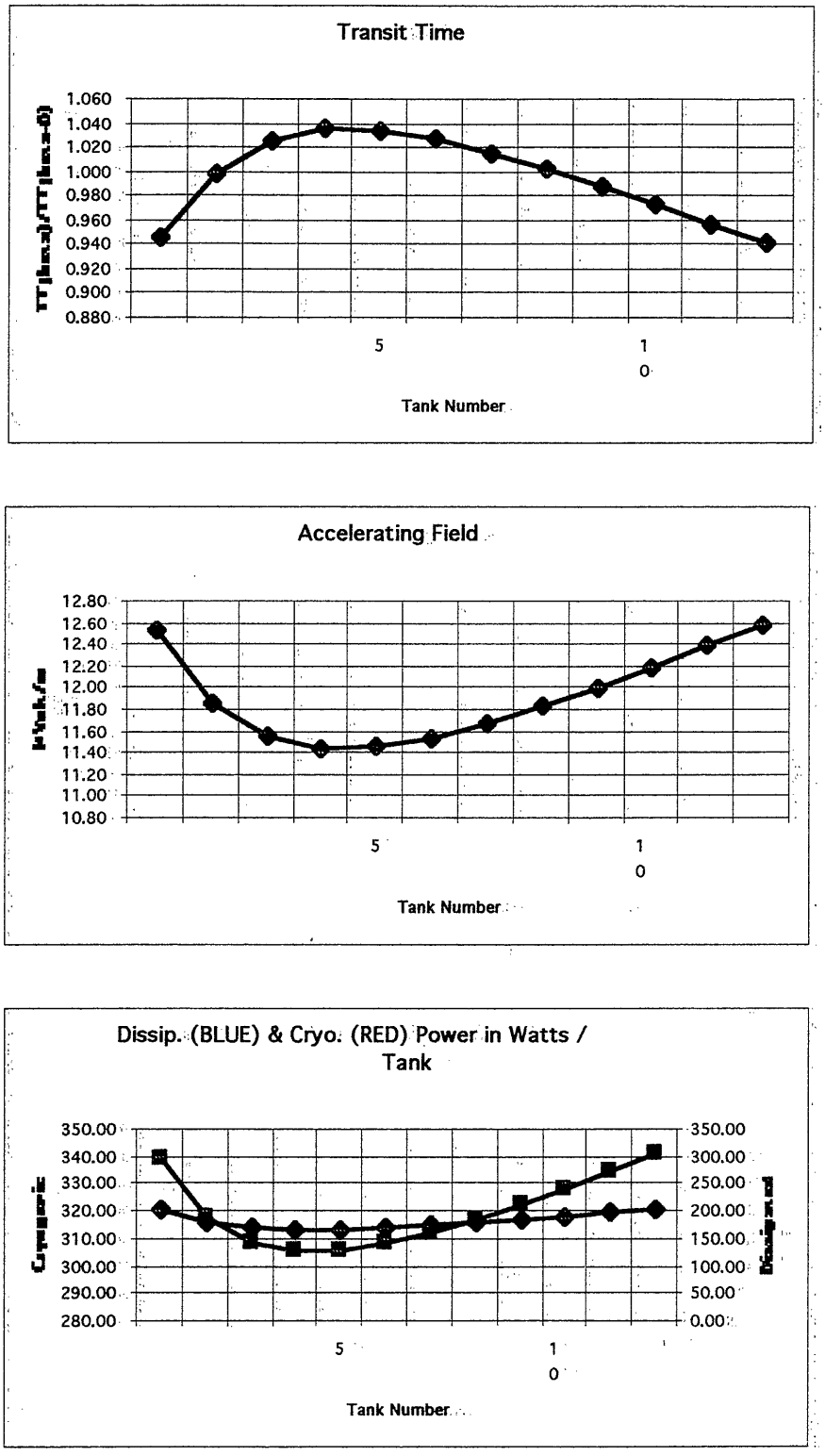

Figure 7. Plots (2) of Behavior vs. *period* (tank) number of MLE Section.

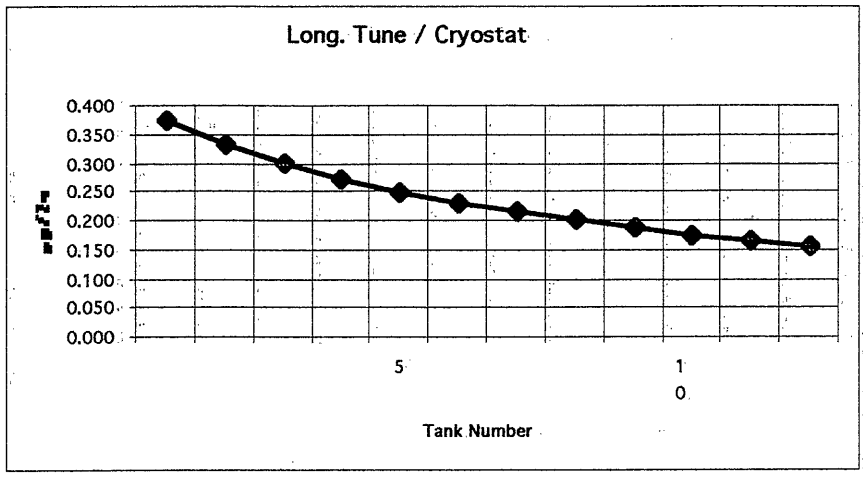

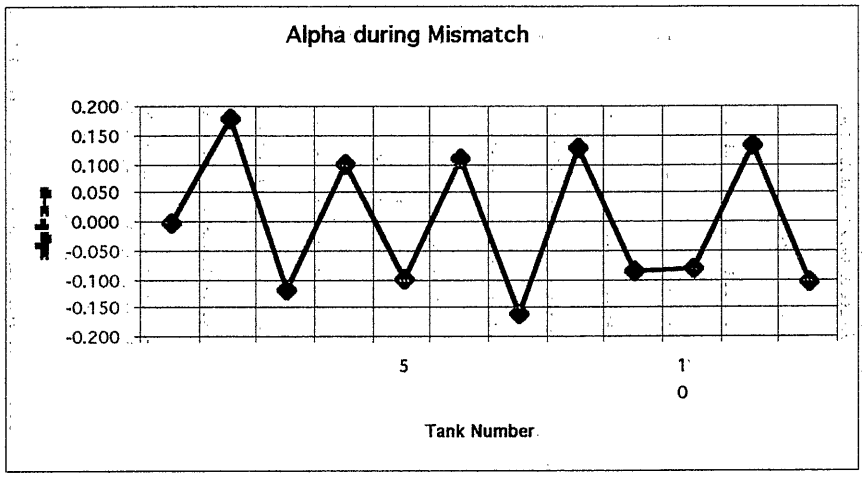

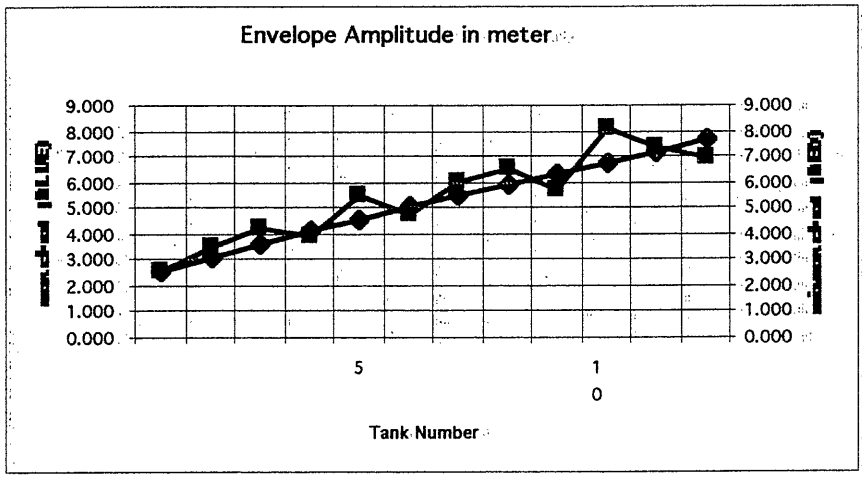

Figure 8. Plots (3) of Behavior vs. *period* (tank) number of MLE Section.

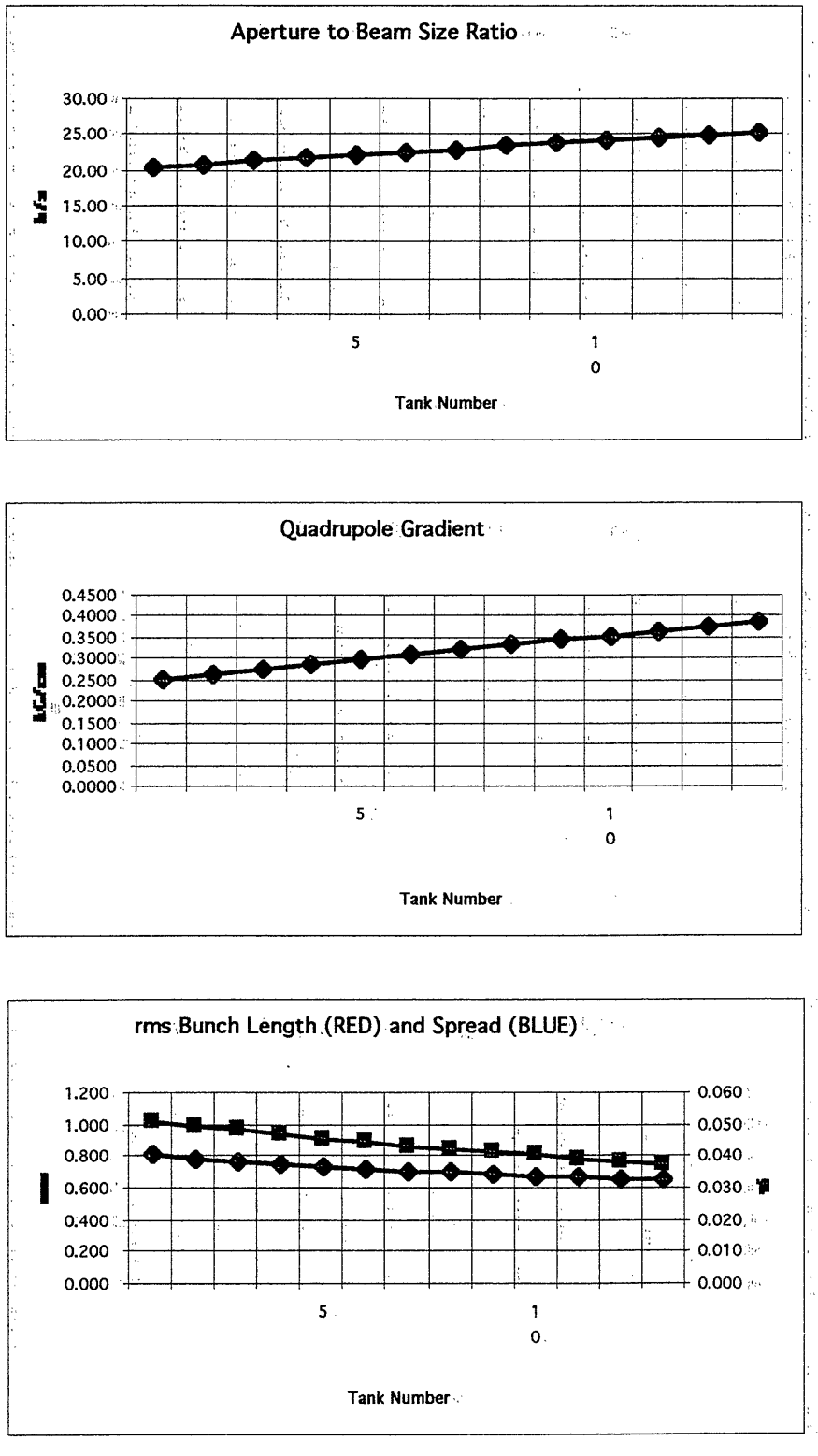

Figure 9. Plots (1) of Behavior vs. *period* (tank) number of MHE Section.

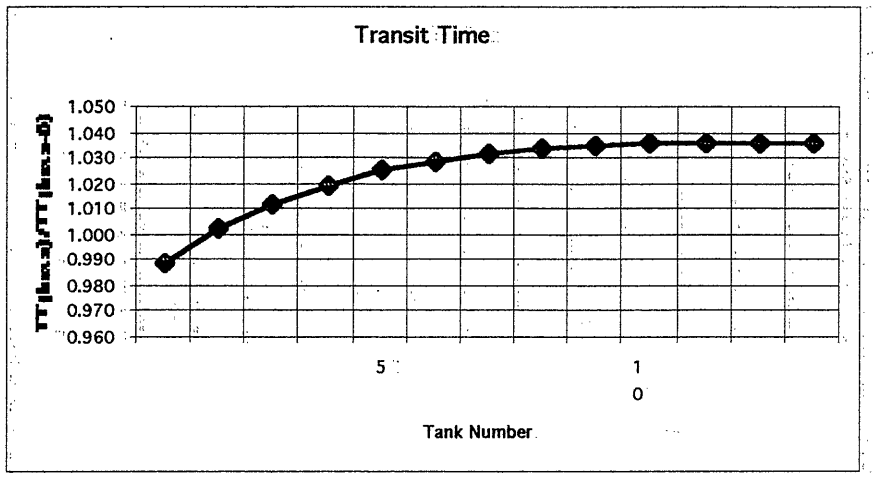

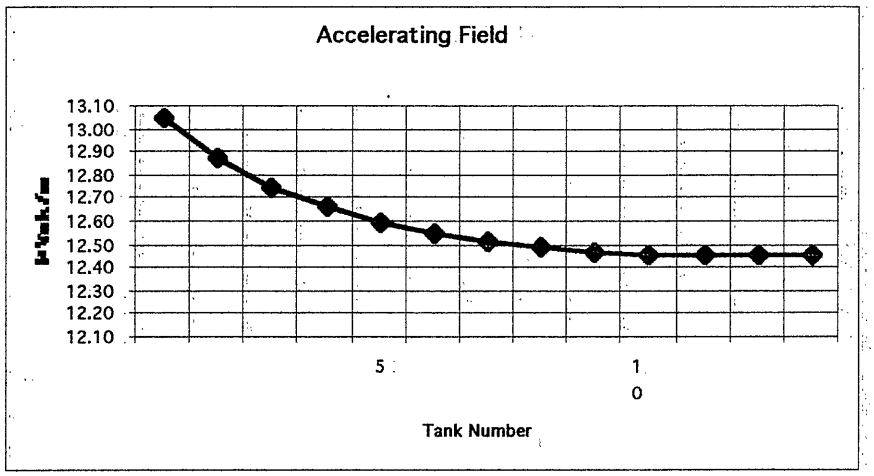

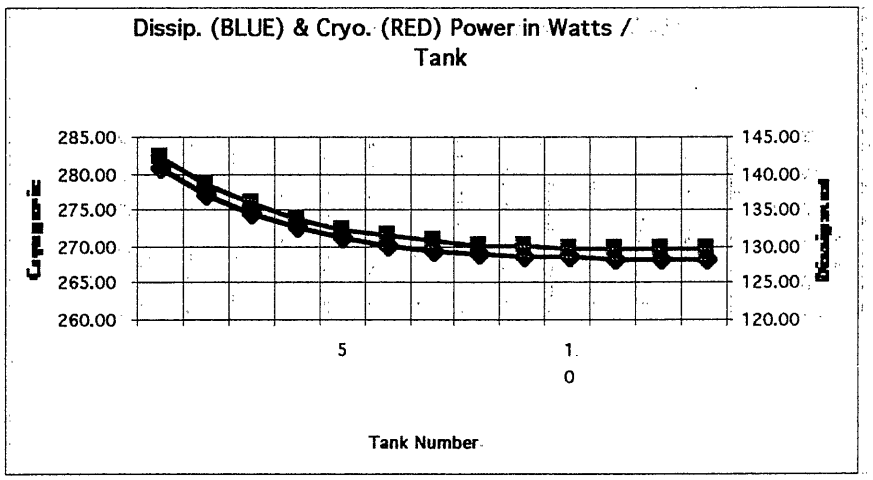

Figure 10. Plots (2) of Behavior vs. *period* (tank) number of MHE Section.

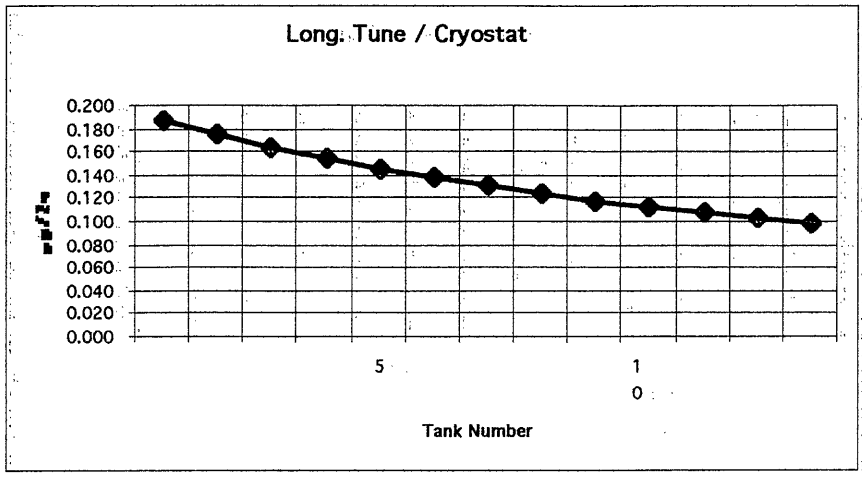

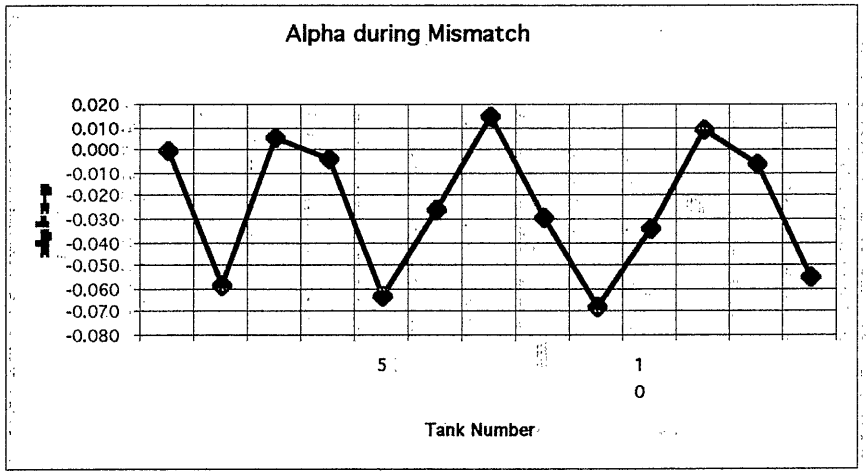

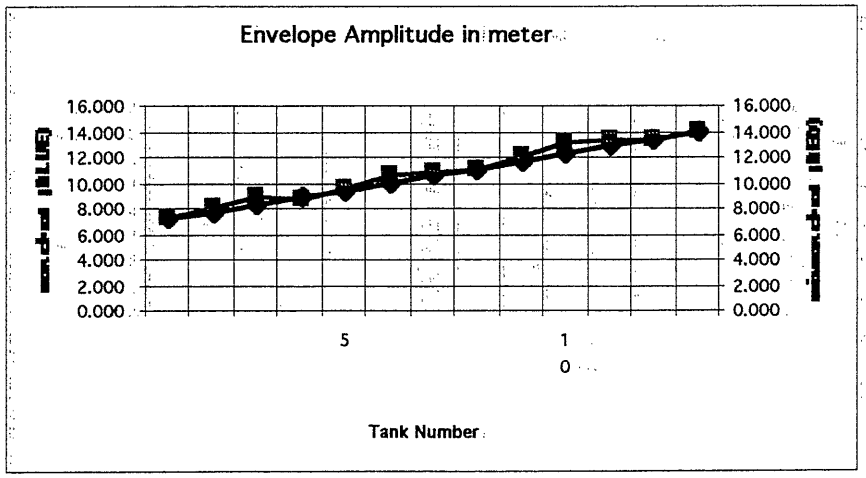

Figure 11. Plots (3) of Behavior vs. *period* (tank) number of MHE Section.

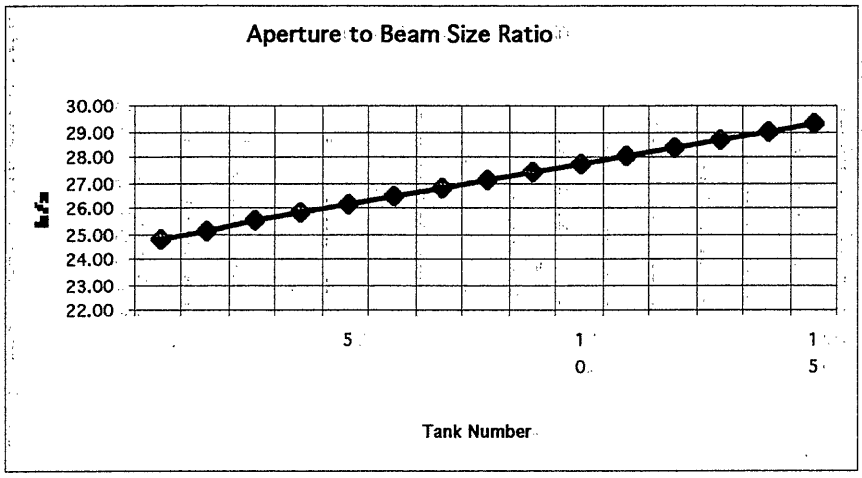

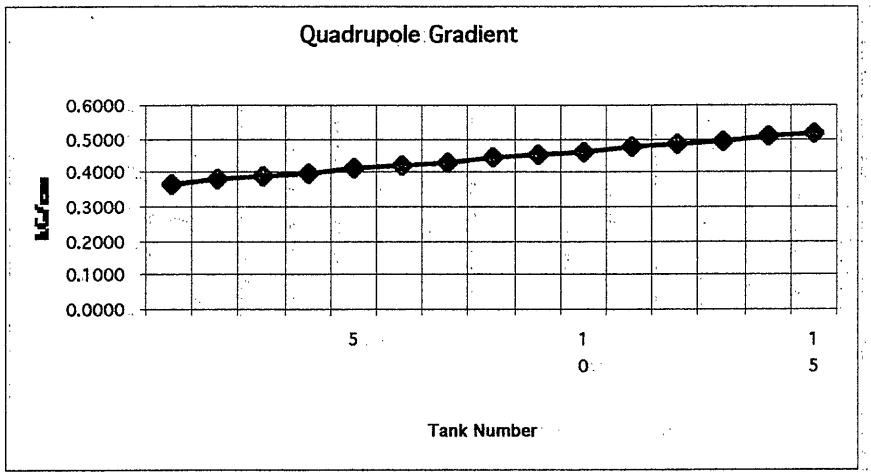

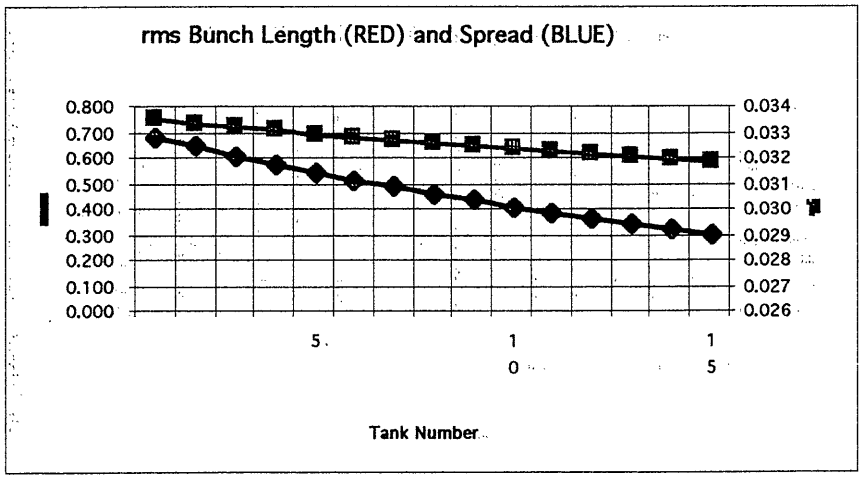

Figure 12. Plots (1) of Behavior vs. *period* (tank) number of HE Section.

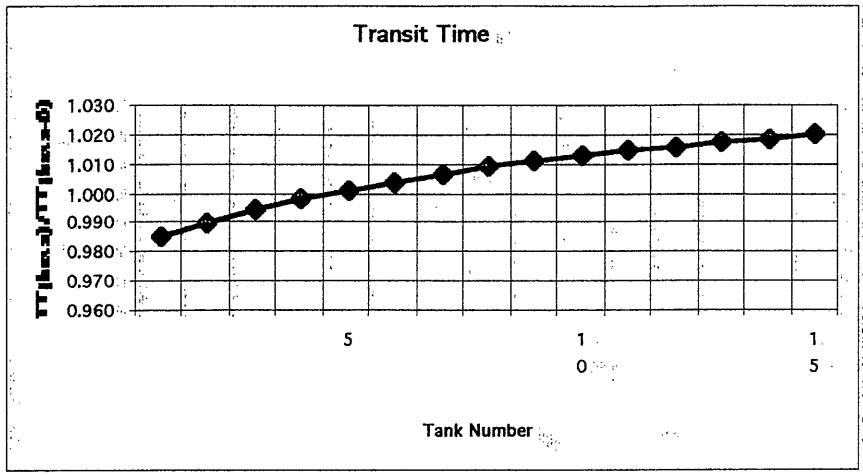

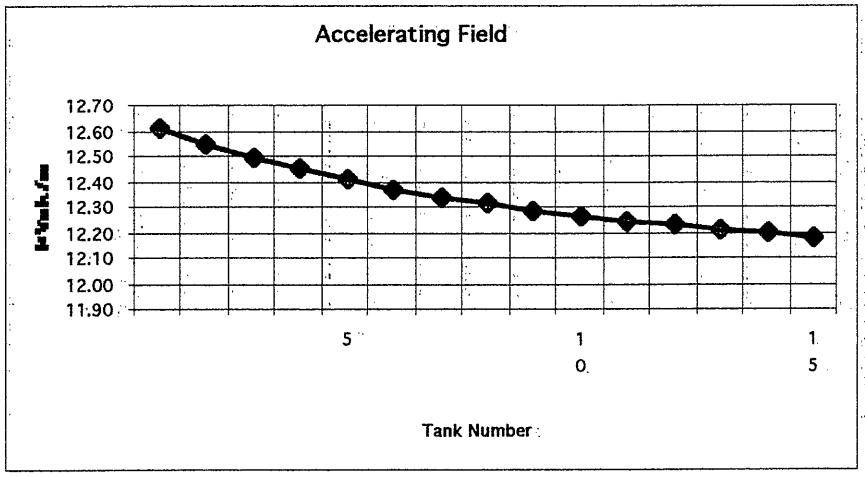

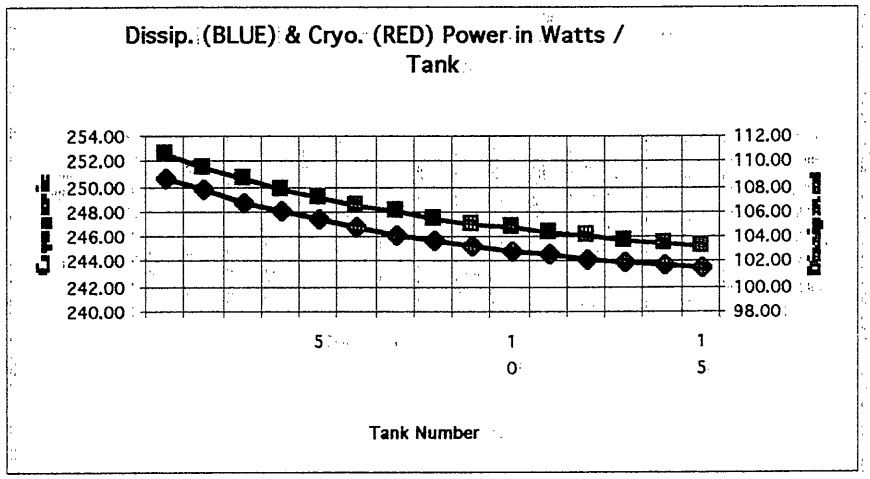

Figure 13: Plots (2) of Behavior vs. *period* (tank) number of HE Section.

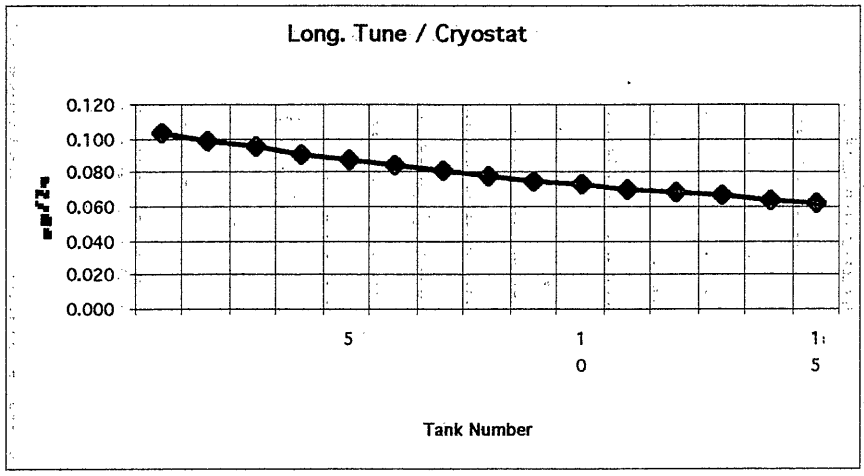

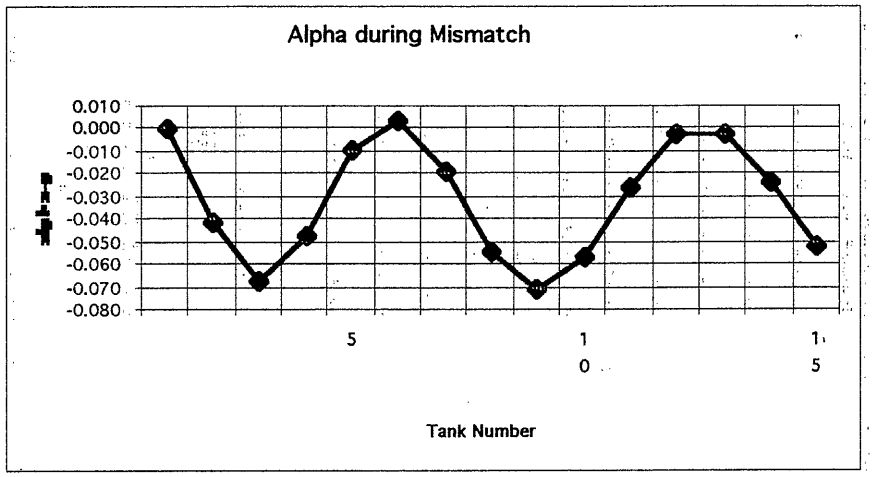

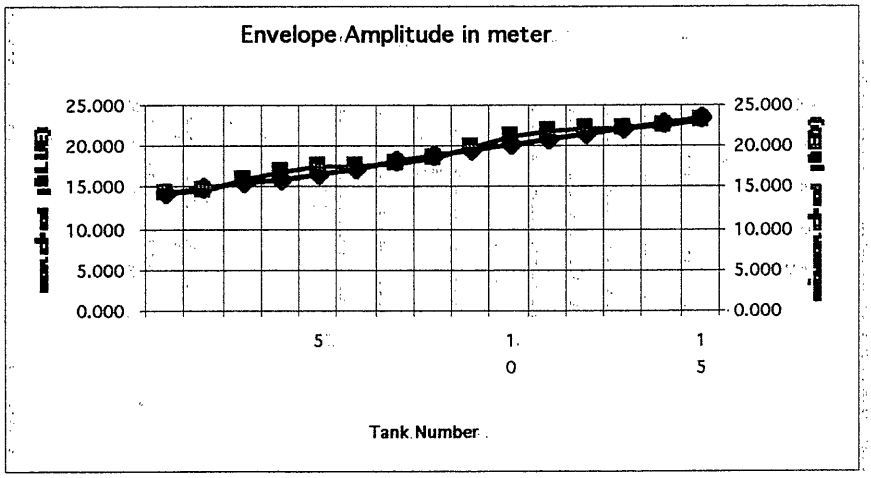

Figure 14. Plots (3) of Behavior vs. *period* (tank) number of HE Section.